

A Realization of Thurston's Geometrization: Discrete Ricci Flow with Surgery*

Paul M. Alsing¹, Warner A. Miller^{2†} & Shing-Tung Yau³

¹ *Air Force Research Laboratory, Information Directorate, Rome, NY 13441*

² *Department of Physics, Florida Atlantic University, Boca Raton, FL 33431*

³ *Department of Mathematics, Harvard University, Cambridge, MA 02138*

Hamilton's Ricci flow (RF) equations were recently expressed in terms of a sparsely-coupled system of autonomous first-order nonlinear differential equations for the edge lengths of a d -dimensional piecewise linear (PL) simplicial geometry. More recently, this system of discrete Ricci flow (DRF) equations was further simplified by explicitly constructing the Forman-Ricci tensor associated to each edge, thereby diagonalizing the first-order differential operator and avoiding the need to invert large sparse matrices at each time step. We recently showed analytically and numerically that these equations converge for axisymmetric 3-geometries to the corresponding continuum RF equations. We demonstrate here that these DRF equations yield an explicit numerical realization of Thurston's geometrization procedure for a discrete 3D axially-symmetric neckpinch geometry by using surgery to explicitly integrate through its Type-1 neckpinch singularity. A cubic-spline-based adaptive mesh was required to complete the evolution. Our numerically efficient simulations yield the expected Thurston decomposition of the sufficiently pinched axially symmetric geometry into its unique geometric structure — a direct product of two lobes, each collapsing toward a 3-sphere geometry. The structure of our curvature may be used to better inform one of the vertex and edge weighting factors that appear in the Forman's expression of Ricci curvature on graphs.

PACS numbers: 04.60.Nc, 02.40.Hw, 02.40.Ma, 02.40.Ky

I. RICCI FLOW IN 3D AND ITS APPLICATIONS

Hamilton's Ricci flow (RF) yields new insights into a broad range of problems from Perelman's proof of the Poincaré conjecture to greedy-routing problems in cell phone networks [1–5]. Here the time evolution of the metric $\dot{\mathbf{g}}$ is proportional to the Ricci tensor $\mathbf{R}c$,

$$\dot{\mathbf{g}} = -2 \mathbf{R}c(\mathbf{g}). \quad (1.1)$$

The RF equation yields a forced diffusion equation for the curvature; i.e., the scalar curvature (R) evolves as

$$\dot{R} = \Delta R + 2R^2, \quad (1.2)$$

here Δ is the Laplacian with respect to the metric \mathbf{g} .

The majority of the engineering applications of RF have been limited to the numerical evolution of piecewise linear surfaces [6]. This is not surprising since a geometry with complex topology is most naturally represented in a coordinate-free way by unstructured meshes, e.g. finite volume [7], finite element [8]. The applicability of discrete RF in two dimensions arise from its diffusive curvature properties and from the uniformization theorem for surfaces. Every simply connected Riemann surface evolves under RF to one of three constant curvature surfaces — a sphere, a Euclidean plane or a hyperbolic plane. RF on surfaces is an accepted method for engineering a metric for a surface given only its curvature [6]. However, in three dimensions, it is significantly more complicated. In particular, singularities can form during evolution under RF. In three dimensions the uniformization theorem yields the geometrization theorem of Thurston showing that each closed 3-manifold has a similar, but richer, decomposition into a connected sum of one or more of eight prime 3-manifolds [9, 10]. The diffusive curvature flow in three and higher dimensions together with this classification provides a richer taxonomy than its 2-dimensional counterpart. We believe this more refined taxonomy may prove useful in network classification. Diffusive curvature flow can provide noise reduction in higher dimensional manifolds, and in this direction we are currently exploring a coupling of RF with persistent homology [11]. Finally, the soliton solutions of RF are Ricci flat and are therefore vacuum solutions of Einstein's equations for gravitation. This feature and its connection to the renormalization group make RF with boundary an exciting topic for current research into AdS/CFT models of quantum gravity [12, 13].

* We dedicate this paper in honor of the 80th birthday of David Mumford for his leadership on the subject of computer vision.

† Corresponding Author: wam@fau.edu

II. DISCRETE RICCI FLOW IN 3D

A discrete RF (DRF) approach for three and higher dimensions, referred to as Simplicial Ricci Flow (SRF), has been introduced recently and is founded on Regge calculus [14–16], as well as complementary work in this direction by [17–21]. The equations of SRF are similar to their continuum counterpart and were shown for this model to convergent. Recently, the Rc_e tensor was reconstructed on each edge e of a lattice geometry [23] adhering closely to the approach by Forman [21]. These new DRF equations form a diagonalized set of first-order autonomous nonlinear differential equations in time. It is numerically efficient and highly parallelizable. There is one equation per edge in the lattice geometry,

$$\frac{1}{\ell_e} \frac{d\ell_e}{dt} = -Rc_e = -K_e + \frac{1}{2}R_e. \quad (2.1)$$

In this DRF equation [23]:

1. K_e is the sectional curvature of edge $\ell_e = \overline{v_1 v_2}$ and is given in terms of the sum over all the edges, ℓ_{e_j} that share a common vertex (v_1 and/or v_2) with edge ℓ_e ,

$$K_e = \sum_{e_{v_1}, e_{v_2} \sim e} \frac{1}{2} \left(\frac{\cos^2(\theta_{e_{v_1}}) \epsilon_{e_{v_1}}}{A_{e_{v_1}}} + \frac{\cos^2(\theta_{e_{v_2}}) \epsilon_{e_{v_2}}}{A_{e_{v_2}}} \right).$$

The data structure for this sectional curvature is illustrated in (Fig. 1). It is expressed in terms of the Voronoi areas A_j dual to the edges ℓ_j , the deficit areas ϵ_j of these edges used in Regge calculus [24], as well as the angle θ_j between edge ℓ_e and ℓ_j . Additionally,

2. R_e is the scalar curvature associated to edge ℓ_e , and it is expressed in terms of the average of the scalar curvatures at each of the endpoints of edge $\ell_e = \overline{v_1 v_2}$,

$$R_e = \frac{1}{2} (R_{v_1} + R_{v_2}).$$

The vertex-based scalar curvatures were introduced earlier in Regge calculus, and is a certain weighted sum of the curvatures of the edges meeting a given vertex [25],

$$R_v = \frac{1}{V_v} \sum_{e \sim v} \ell_e \epsilon_e.$$

Here V_v is the dual volume associated with vertex v , and ℓ_e is the length of the edge emanating from vertex v .

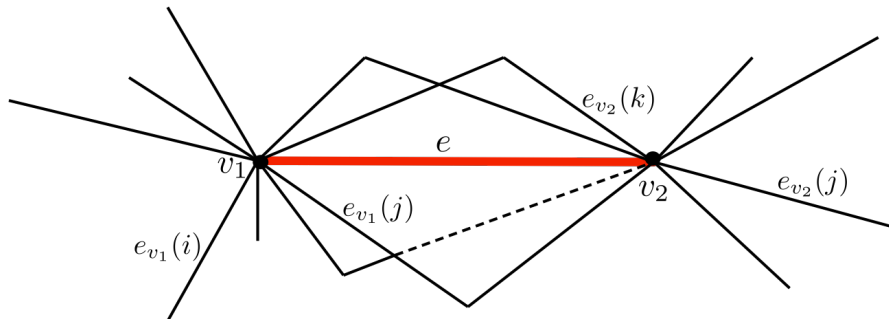


FIG. 1: The data structure of an edge ($e = \overline{v_1 v_2}$) used in our definition of the Forman-Ricci tensor. Included in this data structure are all the edges that share either vertex v_1 or v_2 or both. This data structure is common for both the discrete Ricci flow tensor Rc_{DRF} used here as well as the Forman graph Ricci curvature Rc_F for an edge e in a graph described in Sec. V.

It is the aim of this paper to explore the behavior of these new diagonalized DRF equations in 3-dimensions for a geometry with axial symmetry, and to examine the development of a Type-1 neck pinch singularity through the singularity using manifold surgery techniques. Thus providing the first piecewise linear numerical realization of Thurston’s geometrization using manifold surgery.

III. THE 3D NECKPINCH MODEL

We use the analysis of Angenent and Knopf on the Type-1 singularity analysis of the continuum RF equations as a foundation of this work [26]. They carefully analyzed a class of axisymmetric double-lobed shaped geometries with mirror symmetry about the plane of the neck as illustrated in the top of Fig. 2. The symmetry of this geometry allows us to suppress one of the three dimensions for visualization purposes. In [26] RF was applied to a warped product metric on $I \times S^2$ having the form,

$$g = \underbrace{\varphi(z)^2 dz^2}_{da^2} + \rho(z)^2 g_{can} \quad (3.1)$$

$$= da^2 + \rho(a)^2 g_{can}. \quad (3.2)$$

Here, $I \in \mathbb{R}$ is an open interval,

$$g_{can} = d\theta^2 + \sin^2 \theta d\phi^2, \quad (3.3)$$

is the metric of the unit 2-sphere,

$$a(z) = \int_0^z \varphi(z) dz, \quad (3.4)$$

is the geodesic axial distance away from the waist, and $\rho(a)$ is the radial profile of the mirror-symmetric geometry, i.e. $s = \rho(a)$ is the radius of the cross-sectional 2-sphere at axial distance a from the waist. Angenent and Knopf proved that the RF evolution for such a geometry has the following properties:

1. If the scalar curvature is everywhere positive, $R \geq 0$, then the radius of the waist ($s_{min} = \rho(0)$) is bounded, $(T - t) \leq s_{min}^2 \leq 2(T - t)$, where T is the finite time at which a neck pinch occurs.
2. As a consequence, the neck pinch singularity occurs at or before $T = s_{min}^2$.
3. The heights of the two lobes are bounded from below and, under suitable conditions, the neck will pinch off before the lobes will collapse.
4. The neck approaches a cylindrical-type singularity.

We demonstrated in our earlier work that the SRF equations, for a sufficiently pinched radial profile, reproduced the neck pinch singularity in finite time, and that the SRF evolutions agree with a finite-difference solution of the continuum RF equations for the same profile [27, 28]. However, in our previous analysis we were unable to remove the singularity by manifold surgery and so unable to integrate through the singularity and reproduce the direct product of two collapsing 3-spheres. Furthermore the equations used previously, though proven to converge to the continuum RF equations, form a sparsely-coupled set of autonomous nonlinear first-order differential equations that proved numerically difficult and time consuming to solve.

The discrete model reported here is a piecewise linear (PL) approximation to the double-lobed geometry (e.g. the S^2 cross sections are modeled by icosahedra, and adjacent faces of the icosahedra are connected to each other via frustum blocks) as illustrated in Fig. 3 and described more fully in [14]. Our simulation used 80 cross-sectional icosahedra across the double-lobed profile. We also relaxed the condition of mirror symmetry about the throat and considered asymmetric geometries. This work represents the first non-trivial numerical solution of the new DRF equations, and it is the first DRF integration through a Type-1 singularity via manifold surgery of which we are aware. The results are illustrated in Fig. 4. Our algorithm is numerically efficient, and the illustrative simulation presented here involves the solution of a diagonal set of 159 autonomous nonlinear first-order differential equations. We evolved the left and right lobes for 1682 and 2133 time steps, respectively. We used a time step $\Delta t = 0.25$. There is no longer the need for matrix inversion at each evolution step.

In the next section we describe the initial profile used and the numerical results obtained.

IV. DRF WITH SURGERY: A NUMERICAL REALIZATION OF THURSTON'S GEOMETRIZATION FOR A NECKPINCH GEOMETRY.

We evolved a sufficiently pinched axisymmetric 3-geometry which was given the initial ($t = 0$) radial profile,

$$s_i = 105.15 \left(1 - 0.2 e^{\left(\frac{\xi_i + 0.4}{0.4}\right)^2} - 0.05 e^{\left(\frac{\xi_i + 0.6}{0.3}\right)^2} \cos(\xi_i) - 0.7 \cos(\xi_i)^4 \right), \quad \forall i \in \{1, \dots, n\}, \quad (4.1)$$

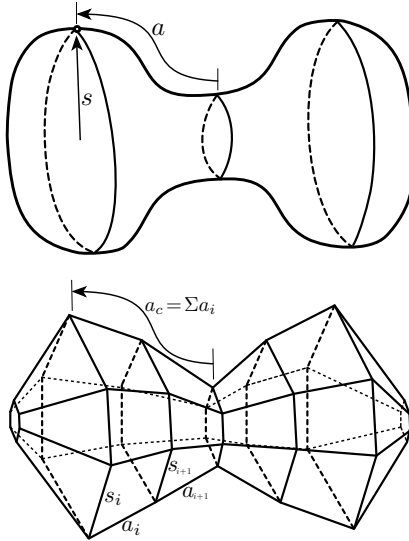


FIG. 2: A two dimensional representation of the 3D neckpinch geometry of Angenent and Knopf (continuum on top, and discrete on bottom). In 3D the continuum cross-sections are 3-spheres and not circles, and in our discrete model the cross sections are icosahedrons and not hexagons. The 3D cells are triangle-based frustum blocks as opposed to the trapezoids depicted in the bottom of the figure. Here the variable a_c measures the proper distance from the equator, and s is the length of the icosahedron edges.

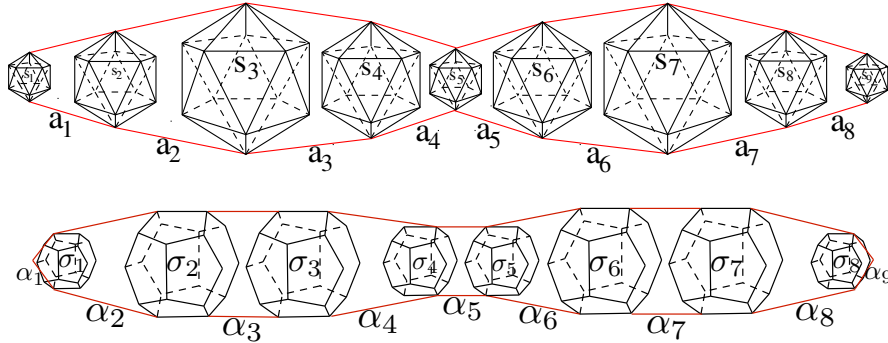


FIG. 3: An illustration of the icosahedron neckpinch geometry for nine cross-sectional icosahedra (top), and its dual dodecahedral lattice (bottom). The lattice is composed of triangle-based frustum blocks, and the dual lattice is composed of pentagonal-based frustum blocks. The expressions for the sectional, scalar, and Ricci curvature uses the dual lattice with its dodecahedral cross sections.

and axial segments,

$$a_i = 100 \sin(\Delta\xi), \quad \forall i \in \{1, 2, \dots, n-1\}, \quad (4.2)$$

where $\xi_i = (n-2i+1)/2$, $\Delta\xi = \pi/(n+1)$, and there are $n = 80$ icosahedral cross-sections. Fig. 4 shows the the initial profile of the lobed geometry in the rectangle to the left along with six other snapshots taken later during the evolution. This initial double-lobed geometry is also illustrated in Fig. 5 and is the outermost curve in the planar embedding. We evolve this surface by numerically solving Eq. 2.1. This geometry evolved to a pinch (third geometry from the left in Fig. 4) at $t = 183.0$. We evolved the equations using a fourth-order Runge-Kutta code with $\Delta t = 0.25$. At every 50 steps in this evolution we remesh the surface using a cubic spline interpolation. This remeshing was necessary to keep the circumcenter inside each frustum block (as described in [27]). Near the singularity $t = 183$ we removed the pinch by manifold surgery yielding the two lobes exhibited in Fig. 5 using the following 4-step procedure:

1. we remove the axial edge a_{45} where the geometry pinched yielding a disconnected left and right lobed geometry each with R^3 topology (the right and left boundaries were removed; respectively);

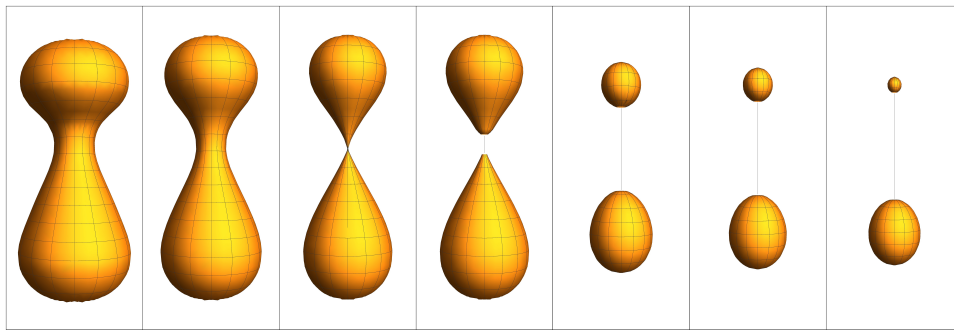


FIG. 4: The RF of a lopsided neckpinch geometry through the Type-1 singularity using surgery and yielding the geometry as a direct product of two 3-spheres. We use axial symmetry of our model to suppress one dimension and the resulting two-lobed geometry can be visualized in Euclidean 3-space (our evolution was fortunately isometrically embeddable in R^3). The middle 3rd and 4th figure occur at the same time ($t = 183.0$) in the evolution. They illustrate the explicit manifold surgery, where the spherical caps (two icosahedrons) are placed on the ends of the left and right lobes. This is the first numerical illustration of Thurston’s geometrization procedure that we are aware of. This surface has 3438 edges, 1580 triangle-based frustum blocks and 960 vertices, although symmetry reduces the number of edges to 80 icosahedral $\{s_i\}$ edges and 79 axial $\{a_i\}$ edges.

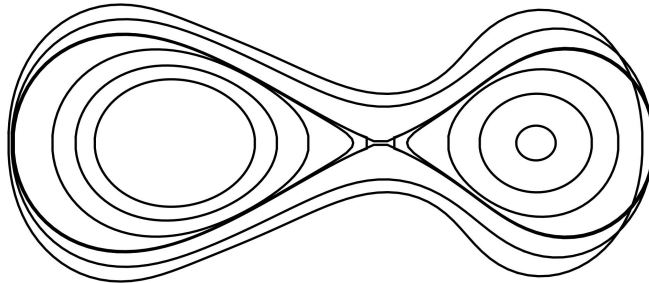


FIG. 5: A 2-dimensional cross section of a lopsided neckpinch geometry evolving under RF through the Type-1 singularity. Surgery yields two disconnected 3D ovoids and each becomes spherical under the RF evolution. The resulting geometry is a direct product of two 3-spheres. As the lobed geometry collapses a pinch occurs at $t = 183$. At this point we remove the axial edges at the pinch and cap each end of the left and right lobe with a new icosahedra. These two surfaces (pre and post surgery) are the 3rd and 4th layers inside the initial surface. After surgery, we remesh both the left and right 3-dimensional ovoids using cubic spline interpolation. This is, to our knowledge, the first numerical realization for PL manifolds of Thurston’s geometrization procedure. This particular surface has 3348 edges, 1580 triangle-based frustum blocks and 960 vertices, although symmetry reduces the number of edges to 80 icosahedral $\{s_i\}$ edges and 79 axial $\{a_i\}$ edges.

2. we capped the left and right lobes by gluing an icosahedra to these open ends with edge length s_{45} and s_{46} thus forming two disconnected 3-dimensional ovoids;
3. we remeshed each of the 3-dimensional ovoids using a cubic spline;
4. finally, we continued evolving using the DRF equations for both of the 3-dimensional ovoids.

A more sophisticated surgery procedure that we illustrate in Fig. 6 was implemented. Here we replace the last three s variables and two a variables with their spherical cap values. Because we found that this more time-consuming and sophisticated approach yields the same results, we chose to use the more austere procedure enumerated above. We evolved these two lobes separately using the Eq. 2.1. Under this flow the curvature uniformized and the lobes each evolved toward a collapsing 3-sphere geometry as shown in the figure. We reproduced expected results with the new DRF equations as shown in Fig. 4 and Fig. 5. In other words, the initial geometry evolved toward a direct product of two constant curvature Thurston geometries, and in particular, as a direct product of two 3-spheres.

This numerical example demonstrates our ability to integrate through a singularity and realize the Thurston decomposition. It also demonstrates that our current approach is numerically more efficient than our earlier formulations.

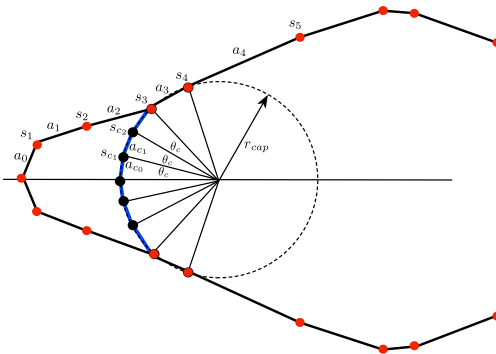


FIG. 6: After the manifold surgery the lobe was closed using a spherical cap with proper matching conditions as illustrated in this figure. This involved reassigning the values to two of the s variables and two of the a values. This procedure offers no essential advantage over the simpler procedure consisting of just capping the surgery with an icosahedron and remeshing.

V. FROM PIECEWISE LINEAR CURVATURE TO GRAPH CURVATURE

While, in this manuscript, we have focused on the discrete Ricci flow of a PL geometry and manifold surgery. Our formulation is based on Forman's curvature construction and can be applied to more general structures, e.g. graphs. It would be interesting to explore the properties of graph curvature flow and determine its utility in characterizing the graph structure, or in its ability to identify and diffuse interesting curvature regions in the graph. To this end, there is considerable interest and pioneering work in applying the Ricci flow techniques to characterize and identify change in dynamic small-world spatial networks [29, 30]. Positive curvature networks stabilize, while negative hyperbolic curved networks expand. The key to these approaches is a measure of the Ricci curvature introduced by Forman [21]. We have identified a striking, but intuitive, relationship between the Forman Ricci curvature Rc_F on graphs and our formulation of the discrete Ricci tensor Rc_{DRF} [22, 23],

$$Rc_F = \frac{1}{2} \left(\frac{\omega(v_1)}{\omega(e)} + \frac{\omega(v_2)}{\omega(e)} \right) - \sum_{e_{v_1}, e_{v_2} \sim e} \frac{1}{2} \left(\frac{\omega(v_1)}{\sqrt{\omega(e)\omega(e_{v_1})}} + \frac{\omega(v_2)}{\sqrt{\omega(e)\omega(e_{v_2})}} \right), \quad (5.1)$$

$$Rc_{DRF} = \frac{1}{2} \left(\frac{R_{v_1} + R_{v_2}}{2} \right) - \sum_{e_{v_1}, e_{v_2} \sim e} \frac{1}{2} \left(\frac{\cos^2(\theta_{e_{v_1}})\epsilon_{e_{v_1}}}{A_{e_{v_1}}} + \frac{\cos^2(\theta_{e_{v_2}})\epsilon_{e_{v_2}}}{A_{e_{v_2}}} \right) \quad (5.2)$$

Here, e is the edge under consideration between two nodes v_1 and v_2 , the edges sharing node v_1 are denoted by e_{v_i} and are each weighted by an appropriate weighting function $\omega(e_{v_i}) \in [0, 1]$ (with $i = \{1, 2\}$), and $\omega(v_i) \in [0, 1]$ is the weighting function for node v_i . The data structure as shown in Fig.1 is identical for both the discrete Ricci tensor and the Forman curvature on graphs. The comparison of these two curvatures for a given simplicial network, e.g. the 600-cell polytope, could sharpen the definition of the vertex and edge weighting function for the Forman curvature. This suggests the following correspondence:

$$\omega(v_j) \longleftrightarrow \cos^2(\theta_{e_j}) \epsilon_{e_j} \quad (5.3)$$

$$\sqrt{\omega(e_j)\omega(e)} \longleftrightarrow A_{e_j} \quad (5.4)$$

We believe this may lead to discoveries characterizing complex networks and work in this direction is already underway [31].

It seems plausible that the set of DRF equations will have an equally rich spectrum of application as does its 2-dimensional counterpart known as combinatorial RF [32]. We therefore are motivated to explore the DRF in higher dimensions so that it can be used in the analysis of topology and geometry, both numerically and analytically, to bound Ricci curvature in discrete geometries and to analyze and better handle higher-dimensional RF singularities [33, 34]. The topological taxonomy afforded by RF is richer in 3D than in 2D. In particular, the uniformization theorem says that any 2-geometry will evolve under RF to a constant curvature sphere, plane or hyperboloid, while in 3-dimensions the curvature and surface will diffuse into a connected sum of eight distinct prime manifolds [9]. We ask is there a similar uniformization/geometrization theorem for 2D/3D spatial networks?

Acknowledgements

We wish to thank Rory Conboye and Matthew Corne for stimulating discussions and for their work. We thank Rory Conboye for his help in reformulating the Forman-Ricci flow equations in their current numerically-efficient form. PMA would like to acknowledge support of the Air Force Office of Scientific Research. We wish to thank the the Information Directorate of the Air Force Research Laboratory and the Griffiss Institute for providing us with an excellent environment for research. This work was supported in part through the VFRP and SFFP program, as well as AFRL grant #FA8750-15-2-0047. Any opinions, findings and conclusions or recommendations expressed in this material are those of the authors and do not necessarily reflect the views of AFRL.

-
- [1] R. Hamilton, “Three-manifolds with positive Ricci curvature,” *J. Diff. Geom* **17** (1982), 255-306.
 - [2] H-D. Cao, B. Chow, S-C Chu & S-T Yau, eds., *Collected Papers on Ricci Flow* in Series in Geometry and Topology, Volume 37 (International Press; Somerville, MA; 2003).
 - [3] B. Chow & D. Knopf, *The Ricci Flow: An Introduction*, Mathematical Surveys and Monographs, Volume 110 (American Mathematical Society; Providence, RI; 2004).
 - [4] B Chow, P. Lu & L. Ni, *Hamilton’s Ricci Flow*, Graduate Studies in Mathematics, Volume 77 (American Mathematical Society; Providence, RI; 2006).
 - [5] B. Chow, S-C Chu, D. Glickenstein, C. Guenther, J. Isenberg, T. Ivey, D. Knopf, P. Lu, F. Luo & L. Ni, *The Ricci Flow: Techniques and Applications, Part 1: Geometric Aspects*, Mathematical Surveys and Monographs, Volume 135 (American Mathematical Society; Providence, RI; 2007).
 - [6] X. Yu, X. Yin, W. Han, J. Gao & X. Gu, “Scalable routing in 3D high genus sensor networks using graph embedding,” *INFOCOM 2012*: 2681-2685; Y. Wang, J. Shi, X. Yin, X. Gu, T. F. Chan, S-T Yau, A. W. Toga & P. M. Thompson, “Brain surface conformal parameterization with the Ricci flow,” *IEEE Trans. Med. Imaging* **31**(2) (2012) 251-264. X. Gu, F. Luo & S-T Yau, “Fundamentals of computational conformal geometry,” *Mathematics in Computer Science* **4**(4) (2010) 389-429; B. Chow & F. Luo, “Combinatorial Ricci flows on surfaces,” *J. Differential Geometry* **63** (2003) 97-129.
 - [7] J. Peiro & S. Sherwin, *Finite Difference, Finite Element and Finite Volume Methods For Partial Differential Equations*, in Handbook of Materials Modeling, Volume 1, Methods and Models, Springer, 2005.
 - [8] S. Humphries, Jr., *Finite-Element Methods for Electromagnetism, Field Solutions on Computers* (ISBN 0-8493-1668-5) (Taylor and Francis, Boca Raton, 1997).
 - [9] W. Thurston, *Three-dimensional geometry and topology*, Vol. 1. Edited by Silvio Levy, Princeton Mathematical Series, 35, (Princeton University Press, Princeton, NJ, 1997).
 - [10] G. Perelman, “The entropy formula for the Ricci flow and its geometric applications,” preprint, math.DG/0211159; G. Perelman, “Ricci flow with surgery on three-manifolds,” preprint, math.DG/0303109; & G. Perelman, “Finite extinction time for the solutions to the Ricci flow on certain three-manifolds,” preprint, math.DG/0307245.
 - [11] P. M. Alsing, H. A. Blair, M. Corne, G. Jones, W. A. Miller, K. Mischaikow & V. Nanda, “Topological Signals of Singularities in Ricci Flow,” *submitted to Axioms* (2017).
 - [12] S. Jackson, R. Pourhasan & H. Verlinde, “Geometric RG flow,” (2013) *arXiv:1312.6914*.
 - [13] M. Carfora & S. Romano, “Quantum fluctuations and geometry: from graph counting to Ricci flow,” (2009) *arXiv:0902.2061v3 [hep-th]*.
 - [14] W. A. Miller, J. R. McDonald, P. M. Alsing, D. Gu & S-T Yau, “Simplicial Ricci Flow,” submitted to *Comm. Math. Phys.* (2013); *arXiv:1302.0804v1 [math.DG]*.
 - [15] P. M. Alsing, J. R. McDonald & W. A. Miller, “The simplicial Ricci tensor,” *Class. Quantum Grav.* **28** (2011) 155007 (17 pp).
 - [16] J. R. McDonald, W. A. Miller, P. M. Alsing, X. D. Gu, X. Wang & S-T Yau, “On exterior calculus and curvature in piecewise-flat manifolds,” *paper submitted to J. Math. Phys.* (2012) *arxiv.org/abs/1212.0919*.
 - [17] D. Glickenstein, D. Champion and A. Young, “Regge’s Einstein-Hilbert functional on the double tetrahedron,” *Differential Geom. Appl.* **29** (2011), 109-124, doi:10.1016/j.difgeo.2010.10.001.
 - [18] D. Glickenstein, “Discrete conformal variations and scalar curvature on piecewise flat two- and three-dimensional manifolds,” *J. Diff. Geom.* **87** (2011) 201-238.
 - [19] D. Glickenstein, “Geometric triangulations and discrete Laplacians on manifolds,” *arXiv:math/0508188 [math.MG]*.
 - [20] H. Ge, “Discrete Quasi-Einstein Metrics and Combinatorial Curvature Flows in 3-Dimension,” *arXiv:1301.3398 [math.DG]*.
 - [21] R. Forman, “Bochner’s method for cell complexes and combinatorial Ricci curvature,” *Discrete Comput. Geom.* **29** (2003) 323-374.
 - [22] R.P. Sreejith, K. Mohanraj, J. Jost,2, E Saucan, and A. Samal, “Forman curvature for complex networks,” *J. Stat. Mech.* (2016) 063206, *arXiv:1603.00386v1*.
 - [23] R. Conboye and W. A. Miller, “Piecewise Flat Curvature and Ricci Flow in Three Dimensions,” *Asian. J. Math.* (2016) in press, *arXiv:1603.03113*.
 - [24] T. Regge, “General relativity without coordinates,” *Il Nuovo Cimento* **19** (1961) 558-571.
 - [25] J. McDonald and W. A. Miller, “A geometric construction of the Riemann scalar curvature in Regge Calculus,” *Class.*

Quantum Gravity **25** (2008) 195017.

- [26] S. Angenent & D. Knopf, “An example of neckpinching for Ricci flow on S^{n+1} ” . *Math. Res. Lett.* **11** (2004) 493-518.
- [27] P. M. Alsing, M. Corne, D. X. Gu, S. Lloyd, W. A. Miller, S. Ray and S-T Yau, “Simplicial Ricci flow: an example of a neck pinch singularity in 3D,” *Geom. Imaging Computing* **1**(3) (2014) 303-331.
- [28] P. M. Alsing, M. Corne, W. A. Miller and S. Ray, “Equivalence of simplicial Ricci flow for 3D neck pinch geometries,” *Geom. Imaging Computing* **1**(3) (2014) 333-366.
- [29] M. Weber, J. Jost and E. Saucan, “Forman-Ricci flow for change detection in large dynamic data sets,” *Axioms* **5**(4) (2016) 26 *arXiv:1604.06634v2*.
- [30] M. Weber, J. Jost and E. Saucan, “Characterizing Complex Networks with Forman-Ricci Curvature and Associated Geometric Flows,” *arXiv:1607.08654*.
- [31] R. P Sreejith, J. Jost, E. Saucan & A. Samal, “Systematic evaluation of a new combinatorial curvature for complex networks,” *Chaos, Solitons & Fractals*, **101**:50-67 (2017).
- [32] B. Chow and F. Luo, “Combinatorial Ricci Flows on Surfaces,” *J. Differential Geom.* **63**, no. 1 (2003) 97-129.
- [33] Y. Lin and S-T Yau, “Ricci curvature and eigenvalue estimate on locally finite graphs,” *Math. Res. Lett.* **17** (2010) 343-356.
- [34] D. Knopf, “Estimating the trace-free Ricci tensor in Ricci flow,” *Journal: Proc. Amer. Math. Soc.* **137** (2009), 3099-3103.